Available online at www.sciencedirect.com

jmr&t Journal of Materials Research and Technology

journal homepage: www.elsevier.com/locate/jmrt

Original Article

Effect of weld microstructure on the tensile properties and impact toughness of the naval, marine-grade steel weld joints

Sameera J. Vaikar [a], *Varun Narayanan* [a], *Joshy Chellathu George* [a,b], *T.C. Kanish* [a], *K. Devendranath Ramkumar* [a,*]

[a] *School of Mechanical Engineering, VIT University, Vellore 632014, India*
[b] *Technische Universität München, München, Germany*

ARTICLE INFO

Article history:
Received 26 March 2022
Accepted 19 June 2022
Available online 27 June 2022

Keywords:
Welding
High strength low alloy steel
Microstructure
Notch tensile strength
Impact toughness

ABSTRACT

Pulsed direct current (PDC) gas tungsten arc welding (GTAW) of 12 mm thick plates of naval, marine-grade high strength low alloy steel (HSLA) using ER80S–Ni3 filler metal was investigated. The microstructural characteristics were examined by both optical microscopy and field-emission scanning electron microscopy (FE-SEM) techniques. The fusion zone is comprised of mixed microstructures of acicular ferrite (AF), polygonal ferrite (PF), grain boundary ferrite (GBF), and bainite ferrite (BF) laths in the various welding passes. The yield and tensile strengths of the PDCGTA weld joints were found to be superior to that of the base metal. A joint efficiency of 122% was observed for the weld seams while conducting the notch tensile studies (NTS). The impact toughness of the weld joints was higher than that of the base metal. The tensile and impact properties in the room temperature (RT) conditions were superior due to the formation of acicular ferrite (AF) and bainite ferrite (BF) laths in the weld seam microstructure. A higher toughness value of 173 J and ductile fracture mode was observed when the joints were impact loaded at −40 °C. On the other hand, the brittle cleavage fracture was observed for the joints subjected to impact loading at −196 °C. The impact toughness data indicated that the joints experienced a transition from a ductile to a brittle mode of fracture on lowering the temperature.

1. Introduction

The ship-building construction, offshore and land-based structures, as well as automotive industries, demand the use of micro-alloyed or high-strength low alloy (HSLA) steels for various applications due to their outstanding strength and toughness. In specific, the HSLA steels can considerably improve the load-carrying capacity and safety performance of container ships and are used widely in deck and hatch coaming structures as described by Sumi et al. [1] as well as for making hull and body of warships and submarines [2]. HSLA

* Corresponding author.
E-mail address: deva@vit.ac.in (K.D. Ramkumar).
https://doi.org/10.1016/j.jmrt.2022.06.104

steels are usually low carbon grade steels micro-alloyed with strengthening elements such as Nb, Cu, Ti, V, and Mn. The elements Nb, Ti, and V, form strong carbides/nitrides, which, in turn, hinder the dislocations/movement of grain boundaries. The HSLA/micro-alloyed steels are designed to possess the ferritic microstructure predominantly with a pearlitic phase less than 10% by volume as stated by Mallik et al. [3]. The changes in the microstructure in the weld seams due to reheating passes significantly affect the mechanical properties, and corrosion resistance. Hence, the selection of welding processes/fillers for joining higher thickness HSLA steels should be appropriate. It is reported that on several occasions, multi-pass welding results in associated weld defects, susceptibility to cold cracking, and residual stresses [3].

Pamnani et al. [4] compared the microstructural features and mechanical integrity of HSLA steel joints established from different fusion welding processes. The authors observed the inclusions in the weld regions obtained from submerged arc welding (SAW), shielded metal arc welding (SMAW), flux-cored arc welding (FCAW), and activated flux GTA welding (A-GTAW) processes. Further, the authors reported that the sub-zero impact toughness of all the welded joints was much lower than the base metal. In another study, Pamnani et al. [5] investigated the residual stress distribution in the weld regions of HSLA obtained from SMAW and A-GTAW processes. According to this research, the higher heat input developed in the A-GTAW process modified the microstructure of the weld region and thus results in higher residual stresses. Raghunathan et al. [6] employed both the fusion welding and solid-state welding techniques adopted for joining 5 mm thick plates of HSLA. Although these authors had achieved a significant grain refinement in the fusion region while employing the friction stir welding (FSW) process, the impact toughness of the joints was lower than the ones achieved from the fusion welding process. Fibre laser welding of similar and dissimilar joints of HSLA and dual-phase steels was achieved by Saha et al. [7]. However, these researchers noticed the tensile ruptures in the heat-affected zone (HAZ) of HSLA steel. Recently, Kannan et al. [8] compared the GMA and GTA welds of HSLA grade DMR 249 A for the microstructure and mechanical properties. The authors noticed a considerable enhancement in the mechanical strength and impact toughness of the GTA welds compared to the GMA welds.

It is often stated that the refinement of grains in the fusion zone improves the mechanical properties of the HSLA steels. The utilization of pulsating direct current (PDC) in GTA welding is a promising way of achieving grain refinement, improved hardness, and better mechanical properties. The periodic fluctuation of two currents, namely peak and background, causes changes in the arc forces and leads to continuous changes in the weld pool shape and size. This gives rise to favoring the growth of new grains as stated by Farahani et al. [9]. The PDC approach has been successfully adopted for welding Ni-based alloys: Inconel X750 [10], Inconel 718 [11], Inconel 625- Inconel 718 [12], as well as duplex stainless steels [13]. However, limited scholarly articles are available in the open literature for adopting PDC welding for HSLA, hitherto.

In the current study, 12 mm thick HSLA plates were welded by the PDC GTAW process using ER80S–Ni3 filler metal in multiple passes by providing suitable inter-pass temperature. A detailed examination of microstructural changes caused due to welding was done using optical microscopy and SEM techniques. The structural integrity of the HSLA weld seams obtained from the PDC GTAW method has been systematically assessed using various mechanical tests. A methodical discussion is also made in contrast to the already published reports.

2. Experimental procedures

2.1. Base metal and welding

The as-received base alloy HSLA plates were machined to the rectangular specimens of attributes 200 × 60 × 12 mm. The composition of elements in the base alloy was explored using the optical emission spectroscopy (OES) method. The compositional data of both the filler and the base alloy are presented in Table 1. The diameter of the filler metal ER80S–Ni3 used in the investigation is 2.4 mm. Apart from the compositional matching of ER80S–Ni3 with the base alloy, the joints obtained from this low carbon alloyed steel filler metal exhibit excellent notch toughness at sub-zero temperatures and room temperature (RT) tensile strength. Hence the selection of filler is made by considering all the above. The structural integrity tests have been conducted for the base alloy and the data is shown in Table 2 to compare the properties with the weld seams. Before welding, the base alloy plates were cut to provide the conventional butt weld configuration (Single V-groove) as shown in Fig. 1. The base alloy plates were firmly clamped with the support of grooved copper back-plates for effective dissipation of heat during welding and also to facilitate the flow of back purging gas. At the

Table 2 – Mechanical properties of the HSLA alloy in the as-received condition.

Mechanical property	Unit	Value
0.2% yield strength	MPa	535 ± 6.5
Ultimate tensile strength	MPa	667 ± 8.5
% Elongation	%	36 ± 1.5
Impact toughness at RT	J	244

Table 1 – Chemical composition of the base alloy and filler metal.

Chemical Composition (% by weight)											
Base or Filler Metal	C	Si	Mn	Cr	Mo	Ni	Cu	Fe	P	V	Others
HSLA	0.073	0.235	1.43	0.038	0.015	0.712	0.152	Rem.	0.09	0.039	Al-0.025; Co-0.04; Nb—0.04; Ti—0.017; S-0.002
ER80S–Ni3	0.08	0.58	1.02	0.04	0.01	3.5	0.14	Rem.	0.012	0.002	S—0.01

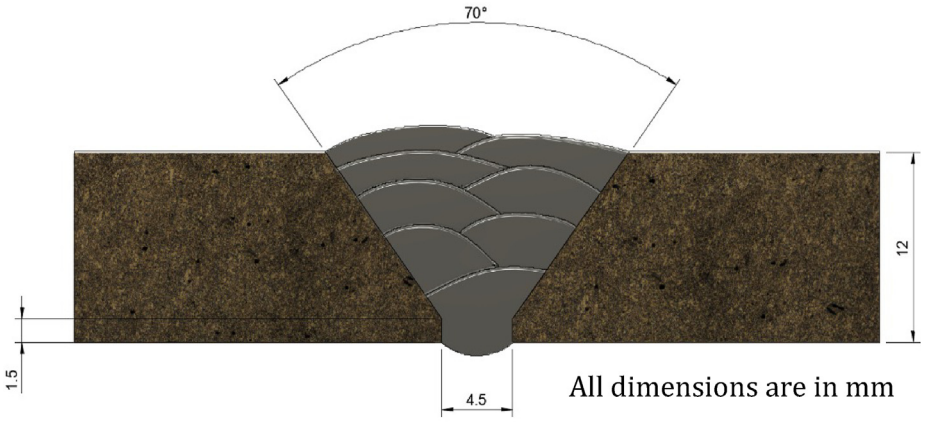

Fig. 1 – Schematic representing the weld configuration and the passes adopted during the PDC GTA welding of HSLA.

end of every welding cycle, the fused region was cleaned using a wire brush to remove the oxides. The welding process conditions adopted for fabricating 12 mm thick joints of HSLA are presented in Table 3. After welding, the HSLA joints were finally cleaned using a wire brush and acetone. The HSLA weld seams were then examined non-destructively using X-ray radiography and ultrasound inspection techniques and the results proved the weld seams are found to be flawless.

2.2. *Metallography and mechanical integrity tests*

The specimens from the HSLA weld seams were machined transversely to the weld direction as indicated in Fig. 2 for executing various experiments using the numerically controlled wire-cut electrical discharge machining [WEDM] technique. The metallurgical assessments using OM and FE-SEM techniques were accomplished on the transverse section samples of dimensions 28 × 10 × 12 mm. The traditional metallographic procedures were adopted to obtain a mirror-like finish on the welded coupons. Further, the surface of the polished sample was chemically etched using 2% of Nital solution to reveal the microstructure across the weld regime. Semi-quantitative, energy dispersive X-ray analysis (EDS) was also performed to identify and characterize the chemical compositions of the phases.

A Vickers microhardness tester (Make: Matsuzawa) was used to explore the hardness trend of the weld seams of HSLA. The computations were executed with a load of 500 gf and 10 s dwell time at every 0.25 mm span along the entire width of the transversely cut specimens from the weld seams. Micro-indentation measurements were computed across the weld seams in the thickness direction associated with various welding passes such as cap, mid-section, and root. ASTM E8/8M–04 standard [14] was used to fabricate the tensile specimens from the weld seams. A 100 kN capacity servo-controlled universal testing machine (UTM) [Instron 8801] was used to estimate the tensile properties of the HSLA weld seams. The crosshead speed of the UTM was kept as 0.2 mm/min to elicit a minimum strain rate on the test samples. The tensile testing was done in triplicate and the average values are reported in the current investigation. ASTM E23:12C standard [15] was adopted to obtain the V-notch test samples in the LT orientation from the HSLA weld seams using WEDM. This LT orientation means that the coupons are placed transverse to the weld direction, with the notch in the middle, and testing takes place across the entire width of the weld seam, covering all passes. These notches were perfectly placed in the joint's middle. CVN impact testing was carried out at sub-zero temperatures of −196, −40 °C, and RT. FE-SEM was used to study the broken surfaces of both the tensile and

Table 3 – Process parameters employed in PDC GTA welding of HSLA.

Parameters	Value
Preheating temperature of the HSLA plates	200 °C
Total Number of Passes	08
Welding Current	Peak Current—196 A and Background Current—110 A for the cap and filling passes Peak Current—170 A and Background current—96 A for the root pass
Voltage	9.65–11 V
Frequency	8 Hz
Duty Cycle	50%
Inter-pass temperature	100–120 °C
Shielding gas	High Purity Argon Gas (99.9%)
Shielding gas flow rate	0.00025 m^3/s (15 Lpm)
Back purging gas	High Purity Argon Gas (99.9%)
Back purging gas flow rate	0.0000833 m^3/s (5 Lpm)

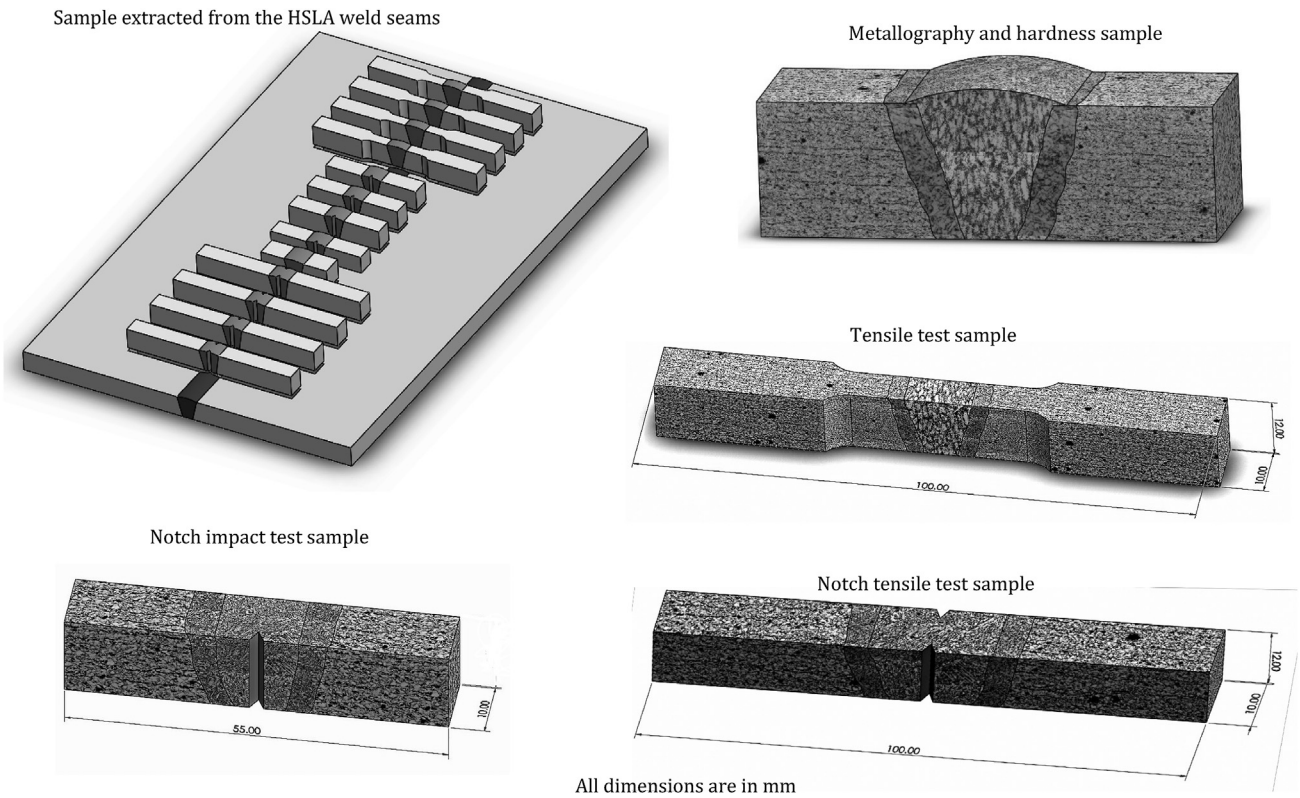

Fig. 2 – CAD models showing the samples extracted from PDCGTA weld seams of HSLA for assessing various metallurgical and mechanical properties.

CVN impact-tested joints to determine and understand the failure mechanism.

3. Results and discussion

3.1. *Metallography analysis*

The HSLA base alloy shown in Fig. 3(a) and (b) is composed primarily of ferrite and traces of pearlite additionally with few inclusions. The optical microscopy image of the base alloy shows that the ferrite is found as polygonal ferrite (PF) predominantly and in a few locations as acicular ferrite. The transverse sectional micrograph shown in Fig. 4 infers that HSLA weld seams achieved from the PDC GTA welding process are free from porosity, cracks, undercut, and other welding defects. The non-destructively testing techniques also assured the soundness of the HSLA joints. The low magnification microscopy images at the various zones of the HSLA weld seams are also embedded in Fig. 4 for better understanding. Both the macrograph and microstructure data attest to the formation of the heat-affected zone (HAZ), which is developed due to the reheating actions sprouted by multi-pass PDC GTA welding. The optical microscopic image at the interface shown in Fig. 5 revealed the occurrence of two distinct HAZs formed adjacent to the fusion boundaries. The region formed adjacent to the weld boundary experiences a higher temperature, which is referred to as a 'coarse-grained heat-affected zone' (CGHAZ). Whereas the region developed closer to the base alloy experiences lower temperatures compared to the former and thus results in a 'fine-grained heat-affected zone' (FGHAZ). The acicular ferrite (AF) is predominated in the microstructure of the CGHAZ along with the BF laths. Similar microstructural aspects were observed by Wan et al. [16]. The presence of alloying additions Nb and Ti in the HSLA could impede the swift grain growth in the HAZ, thus promoting the nucleation and growth of acicular ferrite as pointed out by Yan et al. [17]. It is observed from Fig. 5(c) that several acicular ferrite laths developed in the reconstructed austenitic grains. The lath/plate-like AF colonized the large austenitic grains into smaller zones. The laths of AF when transfigured at elevated temperatures cease the growth of bainite in the ensuing transformation phases [18].

During welding of low carbon, high strength steels, the heating action produces a gradient of austenite grain size in the HAZ, with the coarser grains adjacent to the fusion interface. Imagumbai et al. [19] postulated that when the steels containing a higher number of inclusions are joined by the welding process, the ratio of AF to bainite will be highest in the HAZ and the austenite grain size is also maximum. This theory agrees with the microstructural observation indicated in Fig. 5(c). On the other hand, the FGHAZ contains the equiaxed and polygonal ferrite (PF) along with Ti-rich inclusions seen in Fig. 5(d).

In the PDC GTAW approach, the fusion zone experiences a high heat input during peak current and the solidification

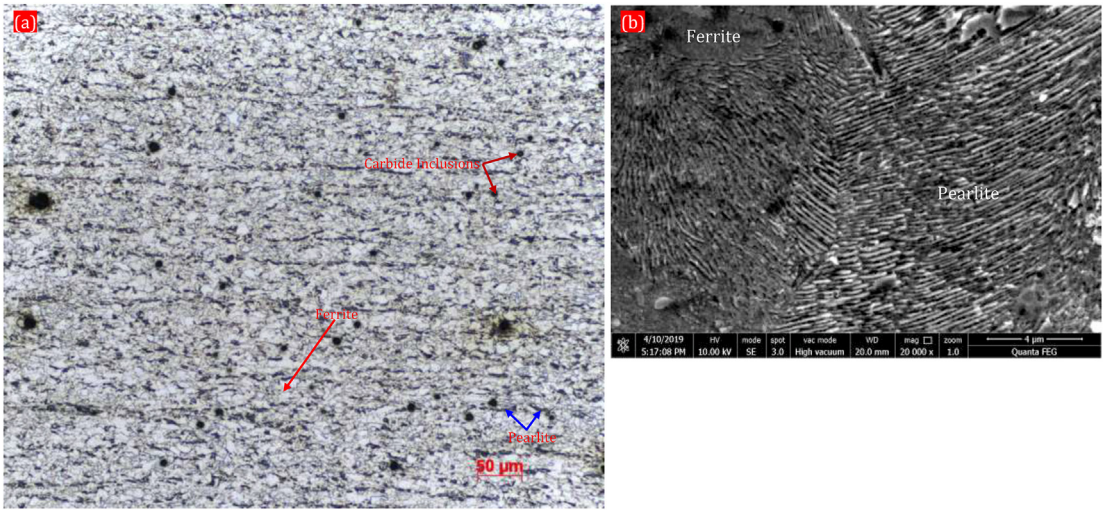

Fig. 3 – (a) Optical microscopy and (b) SEM image of the parent metal of HSLA in the as-received condition.

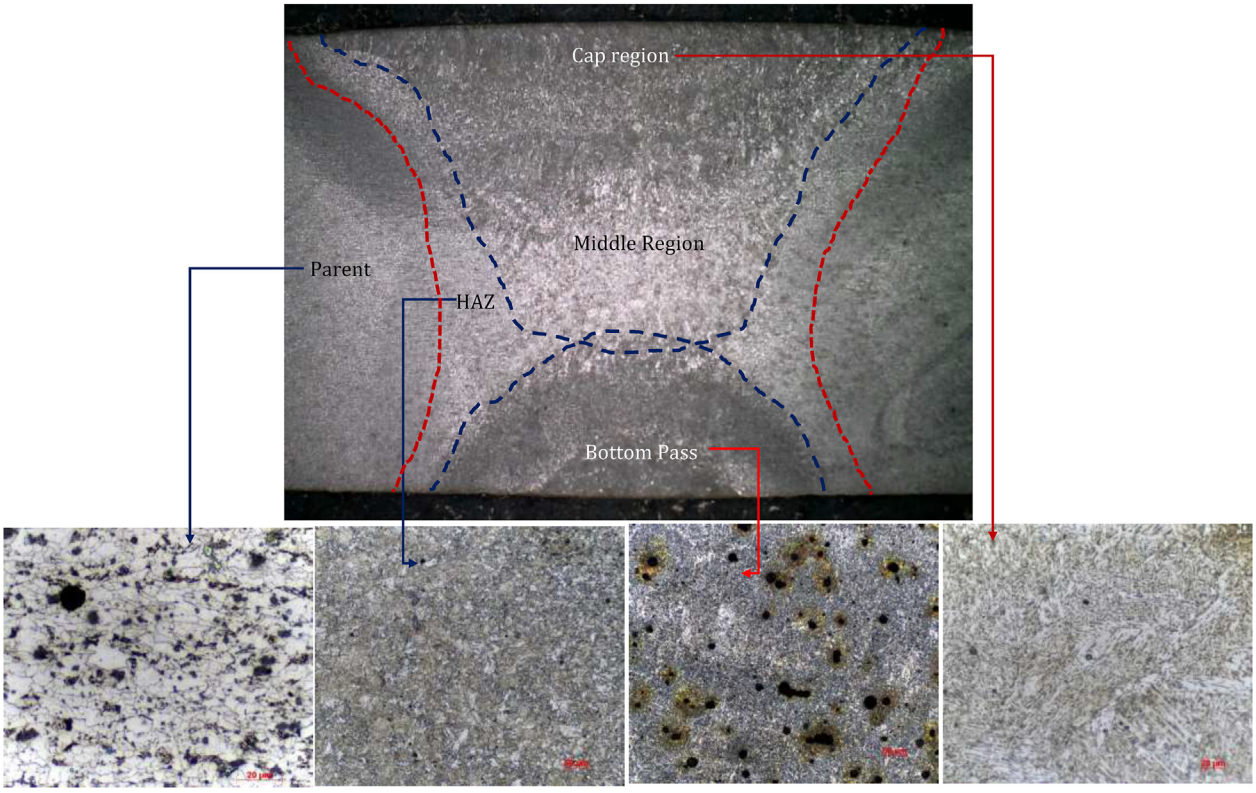

Fig. 4 – Shows the transverse sectional macrostructure (top) and low magnification microscopy images (bottom) of the PDC GTA welds of HSLA steel employing ER80S–Ni3 filler at various zones.

occurs rapidly during the background current and thus experiencing moderate cooling rates. Hence, the microstructure of the weld seams is greatly affected and resulting in the occurrence of both equilibrium and non-equilibrium structures in various passes. The location of the optical microscopy and SEM images at the fusion region of PDC GTA weld seams are shown in Fig. 6(a). The microstructure at the last pass (cap region) of the weld zone is dominated by AF, grain boundary ferrite (GBF), and BF laths. Ti-rich precipitates are also found in the cap region in the acicular ferrite network [Fig. 6(a)–(b)]. The occurrence of AF is achieved in the same temperature range as bainite by the same transformation mechanism

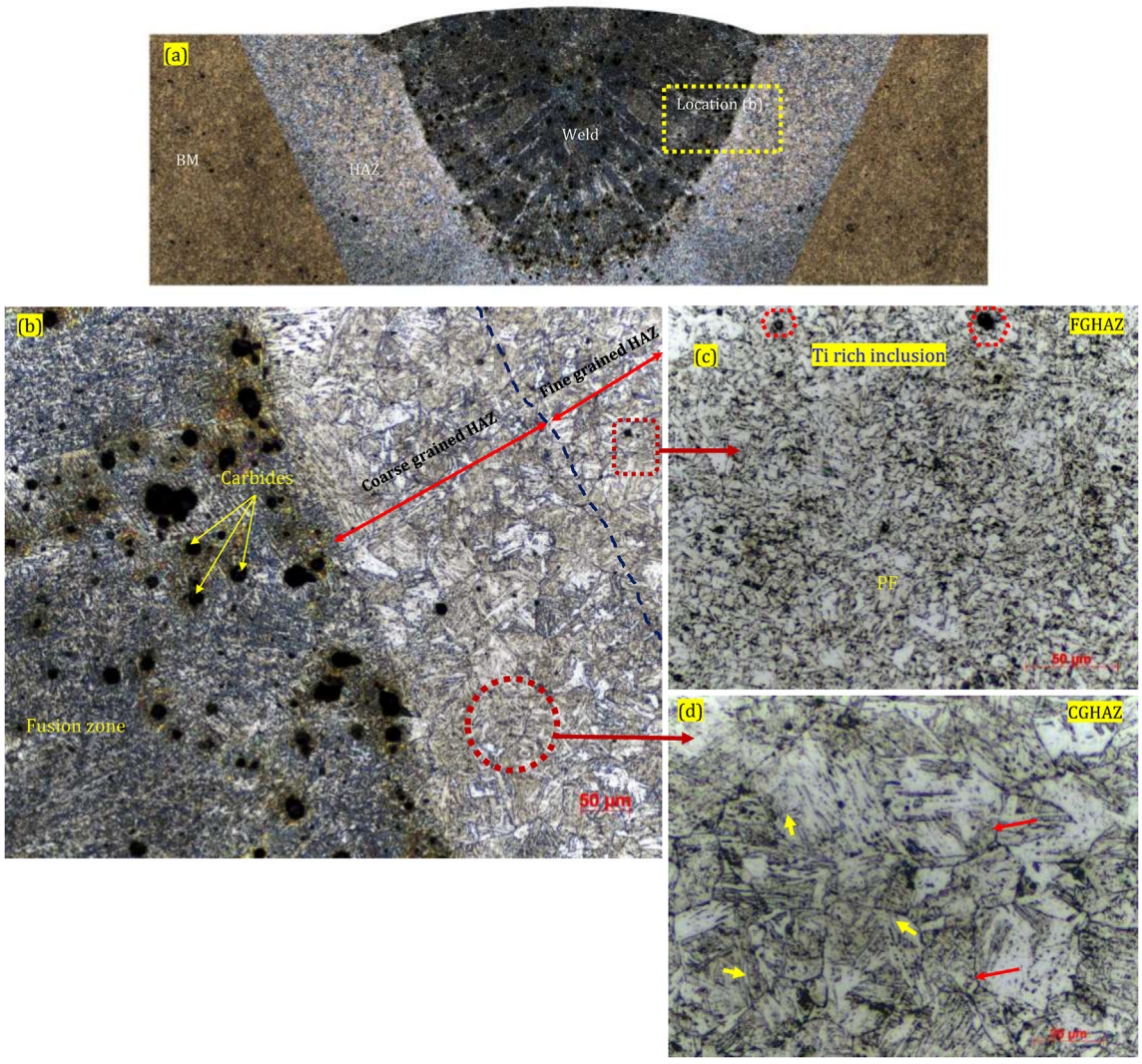

Fig. 5 – (a) CAD image showing the optical microscopic locations; Interface microstructure showing the (b) Inclusions observed in both HAZ and fusion region (c) fine grained HAZ formed closer to the base alloy showing the PF, AF and pearlite features (d) Coarse grained HAZ (Yellow coloured arrows indicate the formation of acicular ferrite and red coloured arrows indicate the austenitic grain boundaries in the CGHAZ).

according to Bhadeshia [20]. The formation of AF is restricted with an increase in the alloying content and a lath bainite structure form. The low efficacy inclusions serve as nucleation sites for the coarse, lath bainite structure to form, as reported by Choi and Hill [21].

As reported by Babu and Bhadeshia [22,23], the nucleation of AF within the austenitic grains demands a greater driving force when compared with bainite, which firstly nucleates at prior austenite grain boundaries. It is to be noted that the growth of AF occurs by a displacive mechanism so there are other effects on the development of microstructure. Thus, the laths/plates like AF are restricted to the grains wherein they grow, for the reason that the coordinated movement of atoms concomitant with this mechanism cannot be continued across grain boundaries. The principal mechanisms of nucleation of intergranular AF could be reasoned as follows: (i) the reduced interfacial energy between ferrite and austenitic phases [18]; (ii) depletion of solute closer to a non-metallic inclusion [24] (iii) thermal strain energy as a result of the different thermal contraction [25] (iv) provision of an inert surface [26]. The various locations of the FZ are further analyzed using a FESEM with the EDS attachment. The spectrum (i) of the EDS analysis shown in Fig. 7(a) indicates a higher amount of Ni, Mn, Si and the spectrum (ii) reveals the presence of Mn, Cr, Co, and Al. Ti-rich precipitates are also dispersed in the FZ as noticed in Fig. 7(b). A higher amount of Ti with small amounts of Al, V, Mn indicates that these inclusions are made of TiO_2, TiS, MnS, SiO_2. The microstructural observations agree with the reports of Kannan et al. [8]. However, there is no dramatic depletion of the quantity of Mn

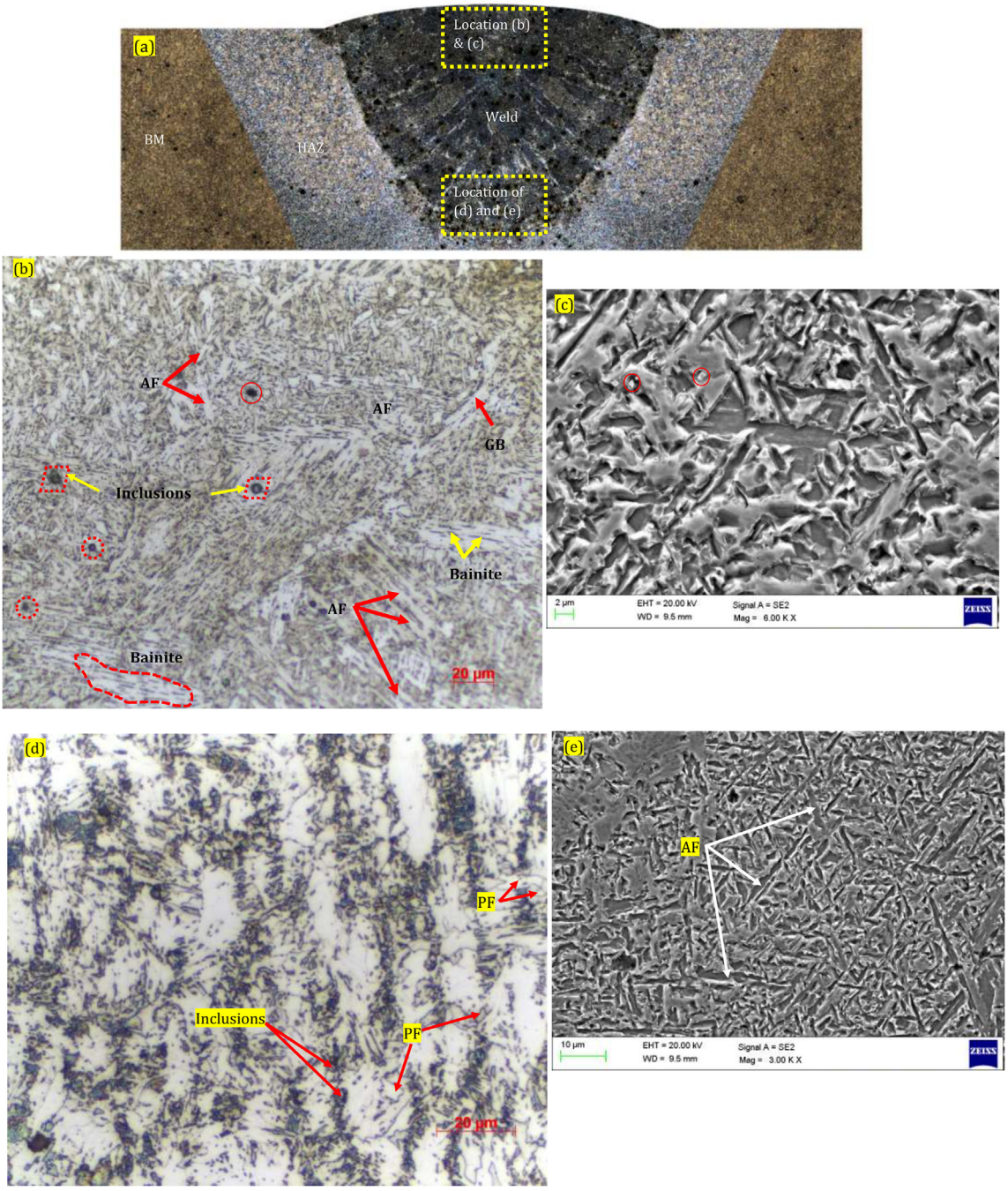

Fig. 6 – (a) CAD model showing the OM locations indicating the weld microstructures; Optical and SEM images representing the microstructures at the weld region showing (b) & (c) Cap and (d) & (e) Root pass of PDCGTA welds of HSLA steel employing ER80S–Ni3 filler.

as reported by these authors. The microstructural data at various locations of HSLA joints are presented in Table 4.

3.2. *Mechanical property assessment*

3.2.1. *Micro-hardness*

The micro-hardness profiles were obtained at three levels as indicated in Fig. 8 on the transversely sectioned weld samples in three different thickness ranges from the top of the weld. The data elucidates that the average micro-hardness in the FZ is higher than the base alloy (209 HV). The changes in micro-hardness data relative to welding pass in different thickness ranges are noted and given in Table 5. It is evident from the data that the root region divulges a higher hardness (297 HV) compared to other regions. It is attributed to the occurrence of AF and BF laths in

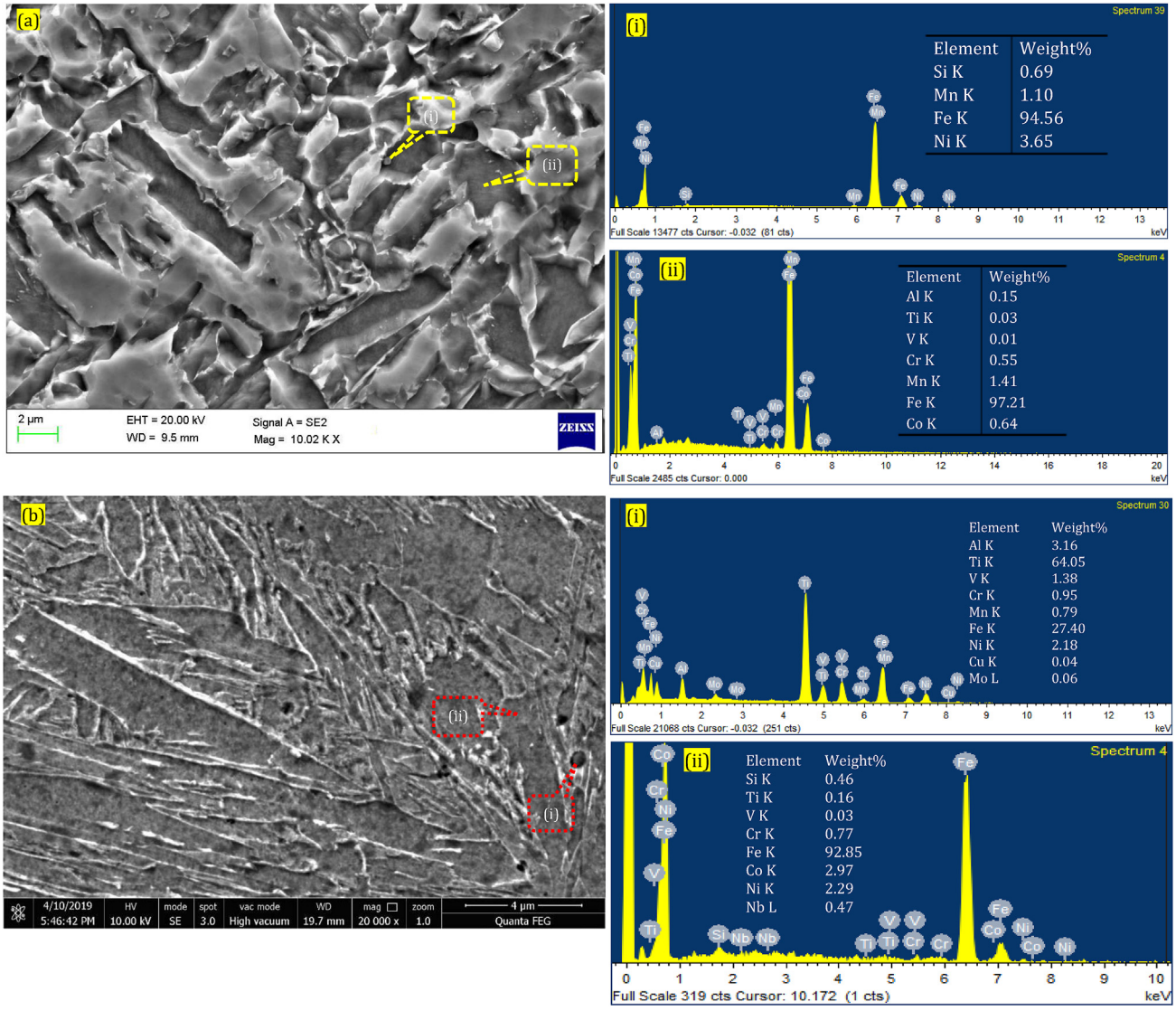

Fig. 7 – (a) and (b) FE-SEM/EDS analysis at the weld region of PDCGTA welds of HSLA steel employing ER80S–Ni3 filler.

the root region, and refined grain growth due to the pulsating current. Similarly, the average hardness reported in the HAZ is found to be 229 H V. It is a fact that during fusion welding, the cooling rates at the HAZ are found to be lower than the weld region, and hence the formation of bainite occurs. Consequently, more carbon atoms are rejected into the remaining austenite phase, thus resulting in a greater hardness. A minor decrease in the hardness adjacent to the fusion boundary line i.e., in the CGHAZ is reasoned to the coarser grains. The occurrence of massive amounts of PF, a soft variant of ferrite imparts a slightly lower hardness of 226 H V in the middle pass compared to the other passes of the weld region. A higher hardness in the FZ is also attributed to the required amount of Mn, Nb, and V alloying elements. Similar remarks are reported by Keehan et al. [27].

Table 4 – Microstructural traits in the various locations of the PDC GTA Welds of HSLA.

Location	Sub-location	Microstructural features
Base alloy	—	Ferrite-Pearlite + Carbide Inclusions
Heat affected zone	—	Acicular Ferrite, Grain Boundary Ferrite, Bainite
Fusion zone	**Cap**	Acicular Ferrite, Polygonal Ferrite and Laths of Bainite
	Middle	Polygonal ferrite, traces of bainite, inclusions
	Root	Acicular Ferrite and Bainite

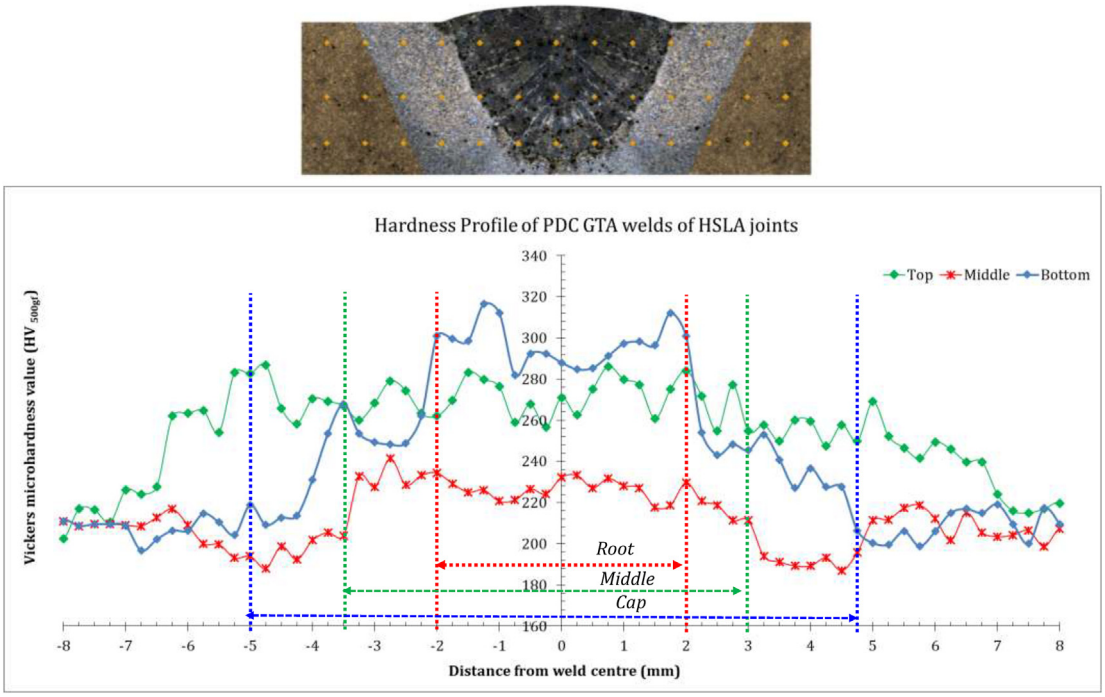

Fig. 8 – Hardness Profiles indicating the various regions of the PDC GTA weld joints of HSLA.

3.2.2. *Tensile properties*

The tensile properties of the base metal and the weld joints of HSLA were assessed in triplicate and the data is provided in Table 2 (for base alloy) and Table 6 (for weld joints). The average 0.2% yield strength (YS) and tensile strength (TS) of the base alloy HSLA are found to be 535 and 667 MPa respectively. Conversely, the PDCGTA weld joints of HSLA exhibit a YS and TS of 583 and 668 MPa respectively. The tensile ruptures were observed in the unaffected base alloy side [Fig. 9(a)] for the joints. The percent elongation of the joints was slightly impoverished compared to the base alloy. However, the YS of the HSLA weld joints is marginally higher than the base alloy bearing ferrite-pearlite microstructure. The higher YS of the HSLA joints might be the cause of grain refinement enacted due to current pulsing and imputed to the precipitation hardening effect because of Nb, Ti, and V. Moreover, the occurrence of a considerable amount of AF and BF laths in the FZ weld microstructure corroborates for great strength. The remarks are on par with Pamnani et al. [4]. The heterogeneous nucleation of AF occurs at the Ti-rich inclusions as stated by Fattahi et al. [28]. The tendency of forming more inclusions is more with Ti present in the fusion region and consequently increasing the nucleation sites for AF. The improvement in the tensile strength is believed to be due to the optimal amount of alloying elements and Ti-rich inclusions in the FZ of HSLA joints. Since the failures were not observed in the weld region, notch tensile studies (NTS) were carried out to estimate the joint strength thereby finding out the joint efficacy of the HSLA weld seams [Fig. 9(b)]. A 1 mm deep notch was evolved on the centre of the weld region to confine the tensile loading in the distinctive stress confining zones. NTS attests that the HSLA weld joints record the tensile strength of 814.5 ± 7.5 MPa. The fractographic features of both tensile and notch tensile tested HSLA joints shown in Fig. 10 connoted the ductile fracture morphologies with the network containing micro and macro-voids and Ti-rich inclusions. The finer distribution of micro-voids in the

Table 5 – Micro-hardness data of the PDC GTA weld joints of HSLA.

Average micro-hardness value (HV_{500gf} or $HV_{4.9033\ N}$)					
Base alloy	HAZ	FZ			
		Cap	Middle	Root	Average
209	229	268	226	297	264

Table 6 – Mechanical properties of the PDC GTA welds of HSLA.

Mechanical Property	Unit	Value
0.2% Yield Strength	MPa	583 ± 8.0
Ultimate Tensile Strength	MPa	668 ± 7.0
% Elongation	%	30.75 ± 1.2
Fracture Location	–	Parent metal
Notch tensile strength	MPa	814.5 ± 7.5
Joint Efficiency	%	122
Impact toughness (Room Temperature)	J	262.5 ± 2.0
Impact toughness (−40 °C)	J	173 ± 3.5
Impact toughness (−196 °C)	J	04 ± 2.0
Physical observation of impact tested sample	–	Ductile

notch tensile tested samples indicated a higher energy absorption before tensile ruptures.

3.2.3. *Impact toughness*

The impact test results indicate that the notch impact toughness of the HSLA weld joints (262.5 J) is superior to the base alloy (244 J) in RT conditions. During RT impact loading, the HSLA joints showed v-notch deformation instead of undergoing complete wreckage [Fig. 11(a)]. The authors believe that the significant improvement in the toughness of the welds could be attributed to the microstructural features containing AF and BF laths in the fusion zone, grain refinement aided by current pulsing, and the precipitation facilitated the strengthening elements. Being the short ferrite needles, the AF forms intra-granularly and is distributed randomly in the FZ microstructure of HSLA joints. The interlocking tendency of AF, in conjunction with its finer grain size, imparts higher impact energy by restricting the propagation of cracks by cleavage. This chaotic, disordered AF morphology restricts the dislocations by providing a pinning effect and thereby improving the strength and toughness of the HSLA joints. Furthermore, the Ti-rich inclusions also contribute to an improvement in RT impact toughness as stated by Pouriamanesh et al. [29]. The study also attests that the impact toughness of the PDC GTA weld joints is found better than the joints established by Ragu Nathan et al. [6] and Venkatesh Kannan et al. [8]. On the contrary, the toughness of the HSLA joints was lowered to 173 ± 3.5 J and 4 ± 2.0 J when operated at sub-zero temperatures of −40 and −196 °C respectively. It is noticed from Fig. 11(b) that at −40 °C, the joints displayed the V-notch deformation confirming a high energy absorption before rupture. On the other hand, the joints were broken into two halves when the joints experienced impact loading at −196 °C [Fig. 11(c)]. The study attests that the PDCGTA joints of HSLA experience a reduction in the toughness of 34.09% and 98.09% when operated at −40 and −196 °C respectively. A ductile to brittle transition is noticed when lowering the temperature from −40 °C to −196 °C. The fractographic features of the impact-tested HSLA joints both in RT and −40 °C conditions also confirm the ductile fracture by manifesting the network of linked micro-voids and dimples shown in Fig. 12(a)–(b). The HSLA joints subjected to an impact loading at −196 °C show a brittle fractured surface, which consists of tearing ridges and cleavage facets. The facets have a river/rock sand-like appearance as revealed from the SEM analysis shown in Fig. 12(c). Also, it is known that BCC metals such as HSLA and other steels are often susceptible to brittle fracture at low temperatures compared to the FCC metals. When the temperature decreases, the mechanism of fracture shifts from ductile failure connoted by upper shelf energy (USE) to brittle cleavage failure, denoted by lower shelf energy (LSE).

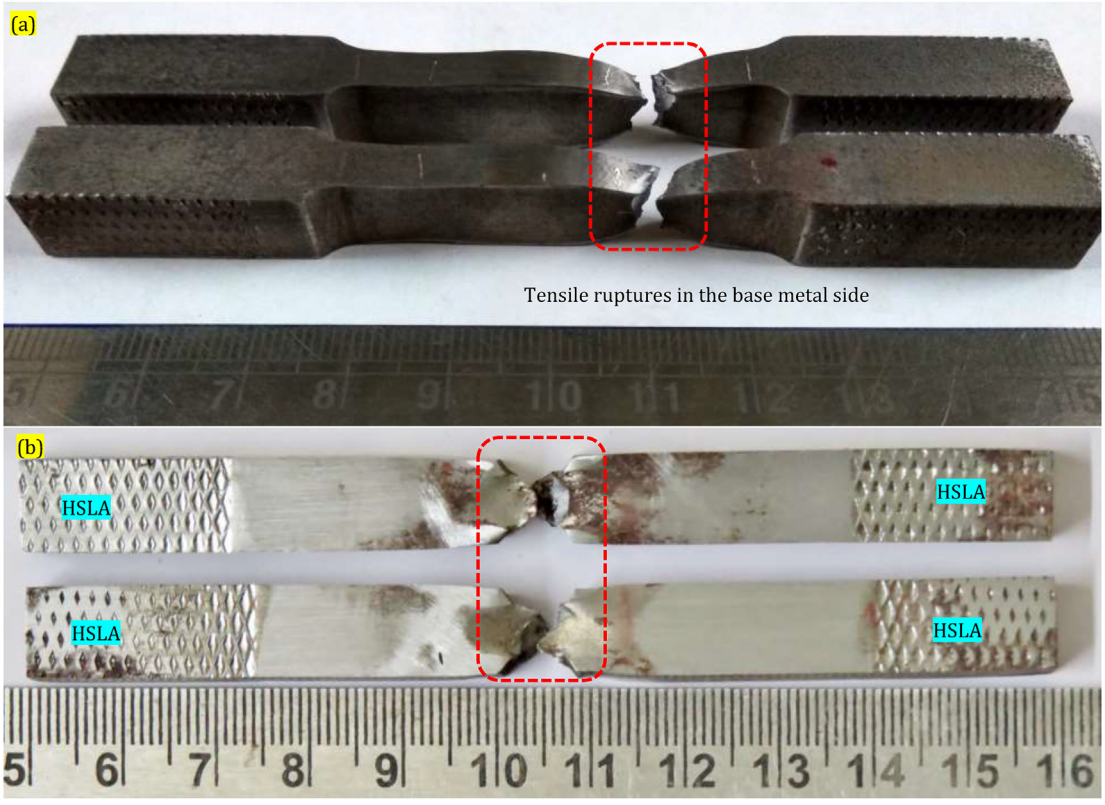

Fig. 9 – Fractured samples of PDC GTA welds of HSLA joints under (a) tensile and (b) notch tensile test.

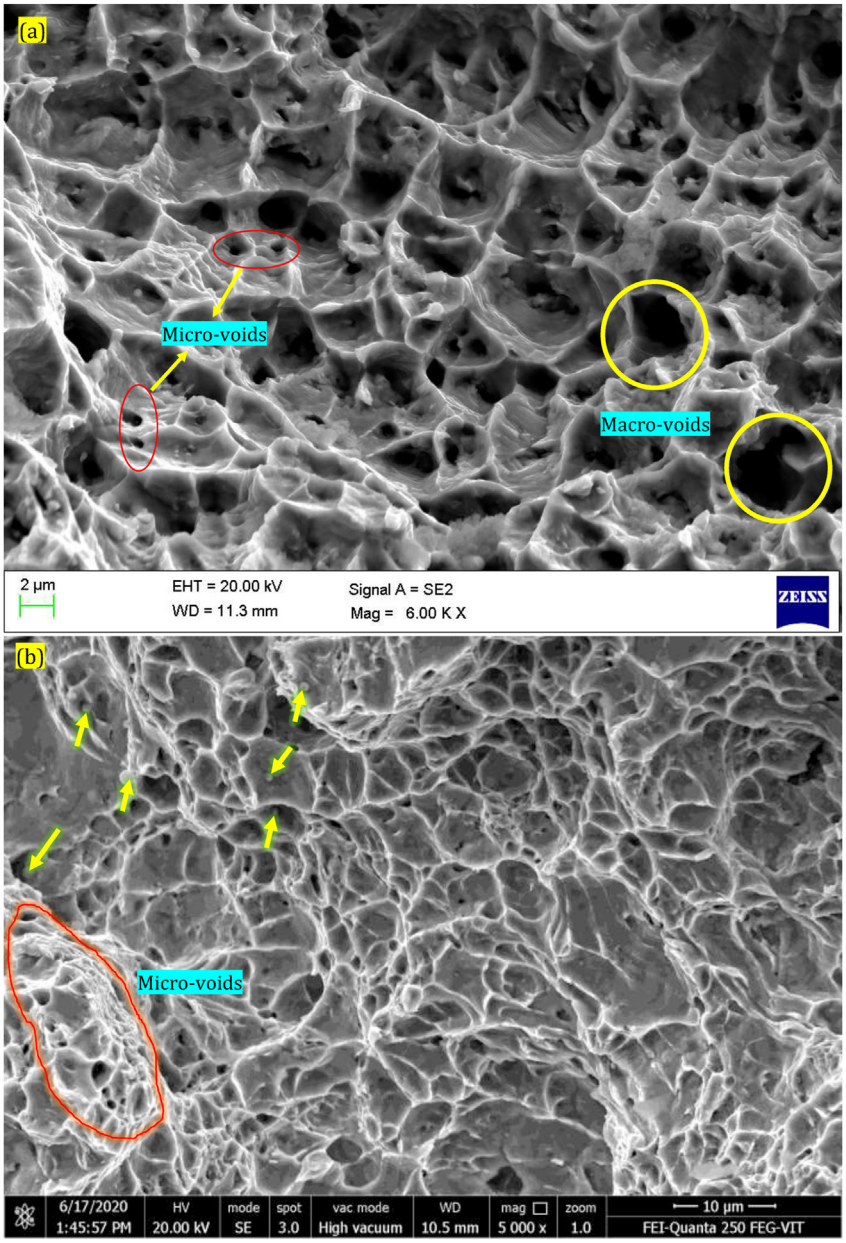

Fig. 10 – FE-SEM fractographic features of the (a) tensile tested and (b) notch tensile tested HSLA joints [arrows indicating the inclusions] respectively.

Armstrong [30] stated that the cleavage fracture mechanism in micro-alloyed steels involves two stages (i) micro-crack nucleation at the regions of stress risers such as carbides, inclusions, hard phases, etc., and (ii) propagation of the developed micro-crack. The authors believe that the existence of carbide precipitation elevates the impact transition temperature and drops the Charpy shelf energy. According to Verdeja et al. [31], the grains oriented in {001} planes parallel to the plane of rolling significantly lower the local cleavage fracture stress on these planes. This, in turn, results in a cleavage behavior parallel to the plane in the rolling during the impact loading, as the {001} planes enhance the fracture due to cleavage in BCC metals. This behavior is liable to form the deep notch-shaped cleavage cracks, which are accountable for the decline in the impact energy, despite the fact that HSLA steel was completely ductile in the upper shelf region. Moreover, the low angle grain boundaries in the BF laths are unable to resist

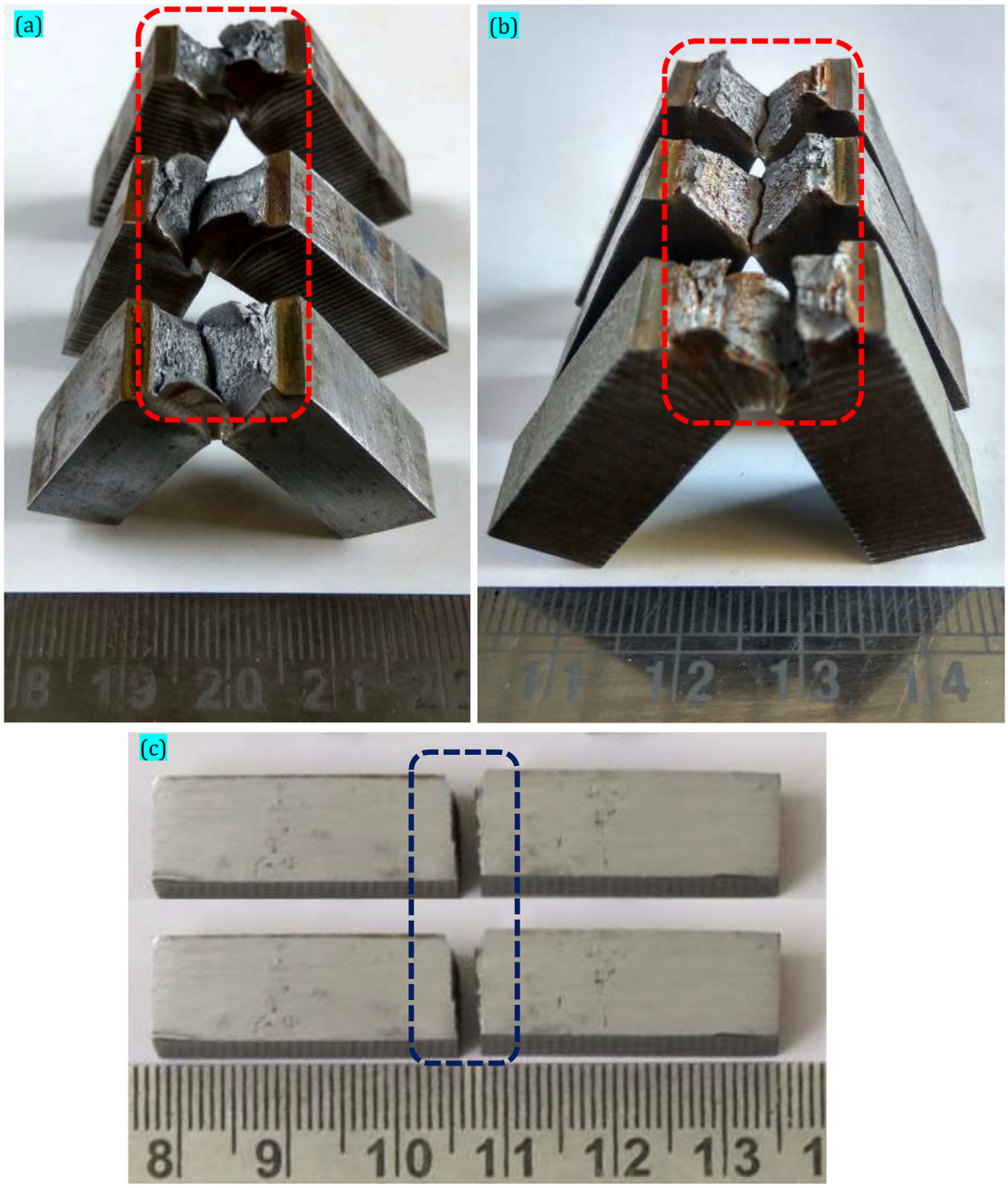

Fig. 11 – Notch impact tested samples of HSLA Joints at (a) Room temperature and Sub-zero temperatures at (b)-40 °C (c) −196 °C respectively.

the crack propagation during impact loading and thus result in cleavage brittle fracture. The EBSD analysis is required to confirm the grain orientation and misorientation angle calculations, which are not presented in the current studies.

In summary, the study attests to the metallurgical investigations and mechanical properties of 12 mm thick HSLA weld joints achieved using E80S–Ni3 filler. In comparison to the specific welding process specifications used, the HSLA joints produced by the PDCGTA welding method had greater tensile strength and impact toughness both in room temperature and sub-zero temperature conditions. The authors believe that the specific findings of the study will be worthwhile for naval applications.

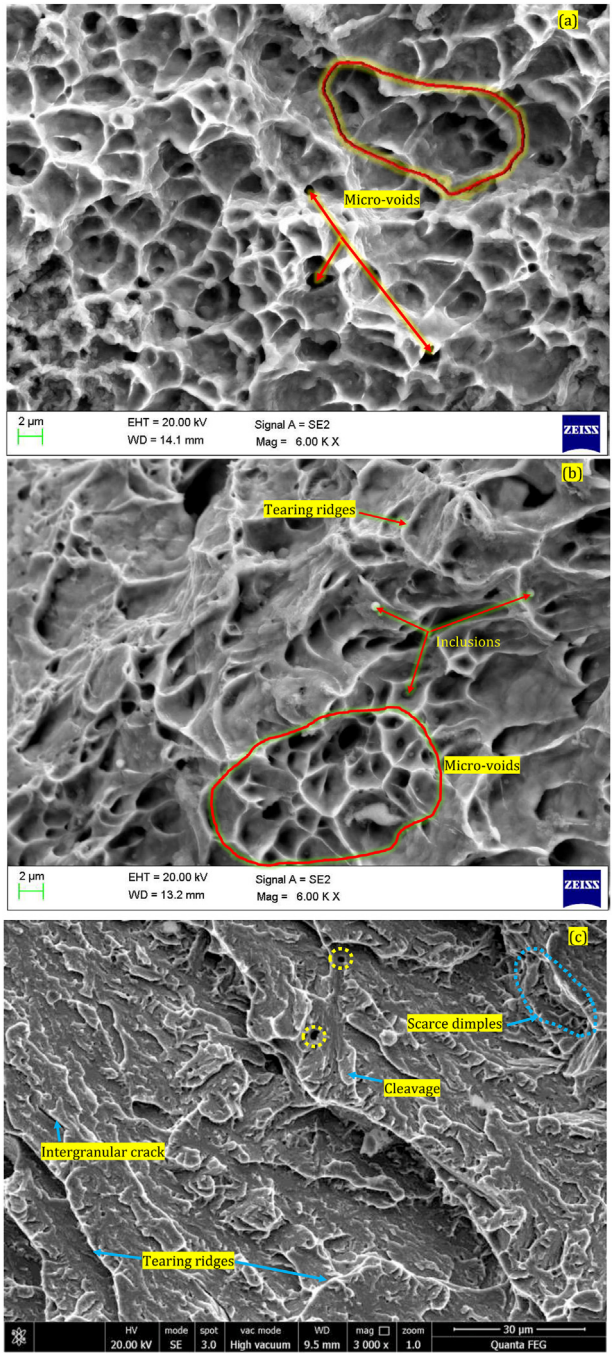

Fig. 12 – SEM fractographic images of the notch impact tested weld seams of HSLA in (a) room temperature and sub-zero temperature conditions (b) -40 °C and (c) -196 °C respectively.

4. Conclusions

The effect of PDC GTA welding and ER80S–Ni3 filler on the fusion zone microstructure and mechanical properties was studied. The major results of the current study can be summarized as follows:

[1] The fusion zone microstructure contains a significant amount of acicular ferrite, polygonal ferrite, grain boundary ferrite, and bainite ferrite laths along with Ti-rich inclusions.

[2] The presence of Ti-rich inclusions promoted the formation of acicular ferrite fusion zone microstructure.

[3] The microstructure studies inferred the occurrence of acicular ferrite and bainitic ferrite laths, which, in turn, resulted in the enhancement of strength and toughness of the joints.

[4] Tensile fractures were noticed in the base alloy side of the joints. The average tensile strength of the joints is 668 MPa. The joint strength and efficiency reported by HSLA joints during the notch tensile test were 814.5 MPa and 122% respectively.

[5] The impact toughness of the HSLA joints is greater than the base alloy. The joints experienced a higher toughness of 262.5 and 173 J respectively when impact loaded at room temperature and −40 °C conditions. The transition from ductile to brittle cleavage fracture is noticed when the temperature is lowered.

Declaration of Competing Interest

The authors declare that they have no known competing financial interests or personal relationships that could have appeared to influence the work reported in this paper.

Acknowledgments

The authors thank the Royal Academy of Engineering, UK for the funding provided as a part of the Industry Academia Partnership Programme (IAPP) [IAPP 18/19–161]. The authors owe a debt of appreciation to Mr. Natarajan, Managing Director, Delta Wear Tech Engineers, Chennai for providing all the necessary facilities for the welding experiments. The authors acknowledge the use of FE-SEM equipment provided by VIT, Vellore, and Sathyabama University, Chennai, and was used to conduct microstructure studies. Our sincere thanks to Microlabs, Chennai, for supporting us with the research.

REFERENCES

[1] Sumi Y, Yajima H, Toyosada M, Yoshikawa T, Aihara S, Gotoh K, et al. Fracture control of extremely thick welded steel plates applied to the deck structure of large container ships. J Mar Sci Technol 2013;18:497–514. https://doi.org/10.1007/s00773-013-0222-5.

[2] Mohammed R, Dilkush, Madhusudhan Reddy G, Srinivasa Rao K. Comparative Studies on microstructure, mechanical and corrosion behaviour of DMR 249A Steel and its welds. IOP Conf Ser Mater Sci Eng 2018;330. https://doi.org/10.1088/1757-899X/330/1/012018.

[3] Mallik S, Minz BS, Mishra B. Production of DMR 249A steel at SAIL, bokaro steel plant. Mater Sci Forum 2012;710:149–54. https://doi.org/10.4028/www.scientific.net/MSF.710.149.

[4] Pamnani R, Jayakumar T, Vasudevan M, Sakthivel T. Investigations on the impact toughness of HSLA steel arc

welded joints. J Manuf Process 2016;21:75–86. https://doi.org/10.1016/j.jmapro.2015.11.007.
[5] Pamnani R, Sharma GK, Mahadevan S, Jayakumar T, Vasudevan M, Rao BPC. Residual stress studies on arc welding joints of naval steel (DMR-249A). J Manuf Process 2015;20:104–11. https://doi.org/10.1016/j.jmapro.2015.09.004.
[6] Ragu Nathan S, Balasubramanian V, Malarvizhi S, Rao AG. Effect of welding processes on mechanical and microstructural characteristics of high strength low alloy naval grade steel joints. Def Technol 2015;11:308–17. https://doi.org/10.1016/j.dt.2015.06.001.
[7] Saha DC, Westerbaan D, Nayak SS, Biro E, Gerlich AP, Zhou Y. Microstructure-properties correlation in fiber laser welding of dual-phase and HSLA steels. Mater Sci Eng, A 2014;607:445–53. https://doi.org/10.1016/j.msea.2014.04.034.
[8] Venkatesh Kannan M, Arivazhagan N, Nageswara Rao M, Madhusudhan Reddy G. Effect of inclusions on microstructure and mechanical behavior of multi-pass welded naval grade steel. Proc Inst Mech Eng Part L J Mater Des Appl 2020;234:1071–83. https://doi.org/10.1177/1464420720927727.
[9] Farahani E, Shamanian M, Ashrafizadeh F. A comparative study on direct and pulsed current gas tungsten arc welding of alloy 617. Growth 2012;2:1–6.
[10] Ramkumar KD, Krishnan SR, Ramanand R, Logesh S, Satyandas T, Ameer A, et al. Structure-property relationships of PCGTA welds of Inconel X750 in as-welded and post-weld heat treated conditions - a comparative study. J Manuf Process 2015;20:1–14. https://doi.org/10.1016/j.jmapro.2015.10.003.
[11] Ramkumar KD, Bhalodi AJ, Ashokbhai HJ, Balaji A, Aravind S, Aravind KM, et al. Effect of Mo-rich fillers in pulsed current gas tungsten arc welding of Inconel 718 for improved strength and hot corrosion resistance. J Mater Eng Perform 2017;26. https://doi.org/10.1007/s11665-017-3009-8.
[12] Ramkumar KD, Abraham WS, Viyash V, Arivazhagan N, Rabel AM. Investigations on the microstructure, tensile strength and high temperature corrosion behaviour of Inconel 625 and Inconel 718 dissimilar joints. J Manuf Process 2017;25:306–22. https://doi.org/10.1016/j.jmapro.2016.12.018.
[13] Yousefieh M, Shamanian M, Saatchi A. Influence of heat input in pulsed current GTAW process on microstructure and corrosion resistance of duplex stainless steel welds. J Iron Steel Res Int 2011;18:65–9. https://doi.org/10.1016/S1006-706X(12)60036-3.
[14] Davis JR, editor. Tensile testing. 2nd ed. Materials Park, Ohio: ASM International; 2004.
[15] ASTM. ASTM E23-12c. Standard test method for notched bar impact testing of metallic materials. West Conshohocken, PA: ASTM International; 2014.
[16] Wan XL, Wei R, Wu KM. Effect of acicular ferrite formation on grain refinement in the coarse-grained region of heat-affected zone. Mater Char 2010;61:726–31. https://doi.org/10.1016/j.matchar.2010.04.004.
[17] Yan W, Shan YY, Yang K. Effect of TiN inclusions on the impact toughness of low-carbon microalloyed steels. Metall Mater Trans A Phys Metall Mater Sci 2006;37:2147–58. https://doi.org/10.1007/BF02586135.
[18] Enomoto M, Inagawa Y, Wu K, Nanba S, Murakami T. Three-dimensional observation of ferrite plate in low carbon steel weld. Tetsu-To-Hagane/J Iron Steel Inst Japan 2005;91:609–15. https://doi.org/10.2355/tetsutohagane1955.91.7_609.
[19] Imagumbai M, Chijiiwa R, Aikawa N, Nagumo M, Homma H, Matsuda S, et al. In: Gray JM, Ko T, Shouhua Z, Baorong W, Xishan X, editors. HSLA steels: metallurgy and applications. Ohio, U. S. A.: ASM International; 1985. p. 557–66.
[20] Bhadeshia HKDH. Bainite in steels: theory and practice. 3rd ed. CRC Press; 2019.
[21] Choi CL, Hill DC. A study of microstructural progression in as-deposited weld metal. Weld J 1978;57(8):232s–6s.
[22] Babu SS, Bhadeshia HKDH. Mechanism of the transition from bainite to acicular ferrite. Mater Trans, JIM 1991;32:679–88.
[23] Babu SS, Bhadeshia HKDH. Transition from bainite to acicular ferrite in reheated Fe–Cr–C weld deposits. Mater Sci Technol 1990;6:1005–20. https://doi.org/10.1179/026708390790189605.
[24] Mabuchi H, Uemori R, Fujioka M. The role of Mn depletion in intra-granular ferrite transformation in the heat affected zone of welded joints with large heat input in structural steels. ISIJ Int 1996;36:1406–12. https://doi.org/10.2355/isijinternational.36.1406.
[25] Enomoto M. In: Nucleation of phase transformations at intragranular inclusions in steel. 4; 1998. p. 115–23.
[26] Zhang S, Hattori N, Enomoto M, Tarui T. Ferrite nucleation at ceramic/austenite interfaces. ISIJ Int 1996;36:1301–9.
[27] Keehan E, Karlsson L, Andre H, Bhadeshia HKDH. Influence of carbon , manganese and nickel on microstructure and properties of strong steel weld metals Part 3—increased strength resulting from carbon additions. Sci Technol Weld Join 2006;11:9–18. https://doi.org/10.1179/174329306X77858.
[28] Fattahi M, Nabhani N, Hosseini M, Arabian N, Rahimi E. Effect of Ti-containing inclusions on the nucleation of acicular ferrite and mechanical properties of multipass weld metals. Micron 2013;45:107–14. https://doi.org/10.1016/j.micron.2012.11.004.
[29] Pouriamanesh R, Dehghani K, Vallant R, Enzinger N. Effect of Ti addition on the microstructure and mechanical properties of weld metals in HSLA steels. J Mater Eng Perform 2018;27:6058–68. https://doi.org/10.1007/s11665-018-3686-y.
[30] Armstrong RW. Material grain size and crack size influences on cleavage fracturing. Phil Trans R Soc A 2015;373:20140124. https://doi.org/10.1098/rsta.2014.0124.
[31] Verdeja JI, Asensio J, Pero-sanz JA. Texture , formability , lamellar tearing and HIC susceptibility of ferritic and low-carbon HSLA steels. Mater Char 2003;50:81–6. https://doi.org/10.1016/S1044-5803(03)00106-2.